Contents lists available at ScienceDirect

Computers in Biology and Medicine

Gait asymmetry assessment through Eigen-Gait components on dissimilarity maps

Lorenzo Hermez [a], Nesma Houmani [a,*], Sonia Garcia-Salicetti [a], Omar Galarraga [b], Vincent Vigneron [c]

[a] SAMOVAR, Télécom SudParis, Institut Polytechnique de Paris, 911120 Palaiseau, France
[b] Movement Analysis Laboratory, UGECAM Ile-de-France, 77170, Coubert, France
[c] Informatique, Bio-Informatique et Systèmes Complexes (IBISC), EA 4526, Université Paris-Saclay, 91020, Evry, France

ARTICLE INFO

ABSTRACT

Motor impairments caused by neurological diseases have an important impact on gait, particularly on the coordination between left and right lower limbs. Deviation from normal gait is often measured to assess this impact on gross motor functions, and to monitor the progress of patients during rehabilitation. The concept of gait dissimilarity map is introduced to represent bilateral raw gait signals, while accounting for their respective spatiotemporal dynamics. A model of gait for the healthy population is constructed through Singular Value Decomposition, considering both lower limbs. The obtained eigenvectors synthesize the symmetry present in gait. Then, by projecting the dissimilarity maps of patients with gait disorders on the space formed by such eigenvectors, we compute their associated Eigen-Gait Asymmetry Index (EGAI) relatively to an average normal gait reference vector. For the knee joint in the sagittal plane, EGAI values of patients are higher (9.73 ±2.16) than those of healthy controls (3.86 ±0.9), reflecting the asymmetry induced by neurological diseases. Patients with hemiparesis show the highest EGAI (10.4 ±1.8), followed by patients with paraparesis (9.9 ±1.8) and patients with tetraparesis (8.6 ±2.5). Indeed, patients with hemiparesis show a more asymmetrical gait since only one side of the body is affected. EGAI for hip, ankle and pelvis joints in the sagittal plane show similar trends. Our innovative method characterizes bilateral gait, enriching traditional unilateral assessments. Our method yields a comprehensive score reflecting both asymmetry and gait deviations, aiming to provide clinicians with an effective and precise monitoring tool.

1. Introduction

Human gait is a complex spatiotemporal activity driven by cyclical movements. It requires the interaction and the coordination between body segments and a coupling of adjacent joints for an effective execution of body displacement. The symmetrical execution of movements between the left and right sides of the body is a functional normative marker [1].

In the healthy population, periodic and symmetric movements of limbs during gait are controlled by the Central Nervous System (CNS). Neurological diseases, such as cerebral palsy, multiple sclerosis, or stroke, relate to a dysfunction of CNS leading to degraded gait quality, impacting gait symmetry [1,2]. This impact is highly variable, according to the pathology and the individual. In hemiparesis, only one side of the body is affected; in paraparesis and tetraparesis, upper and/or lower limbs can be impacted.

Gait quality assessment has considerably evolved in recent years. Advances in acquisition technology as inertial measurement units [3–7] and motion capture systems [8,9] allow recording precise kinematic joint angles for Clinical Gait Analysis (CGA) [3,10–13]. Such joint angles are exploited in CGA to assist clinicians in patients' follow-up by means of quantitative indices [14,15]. Different measures have been introduced to quantify the asymmetry present in pathological gait [16], particularly the Ratio Index (RI) [17] and the Symmetry Index (SI) [18]. The RI quantifies gait symmetry by computing a ratio between global descriptors (e.g. step width or step length [19–25]) of the affected and non-affected limbs. The SI is based on the difference between the descriptors of the affected and non-affected limbs, normalized by a reference value of the given descriptor. The choice of the reference value is not obvious; for this reason, such value is estimated as the average of the descriptor of the left and right sides [16,26]. For both indices, a zero value indicates perfect symmetry. SI and RI indices show

---

* Corresponding author.
E-mail address: nesma.houmani@telecom-sudparis.eu (N. Houmani).

Table 1
Descriptive statistics (mean ± standard deviation) for healthy and pathological populations.

	HC	All patients	HP	PP	TP
Number of individuals	52	45	21	11	13
Number of bilateral cycles	263	212	100	49	63
Female	34 (65%)	14 (31%)	7 (33%)	4 (36%)	3 (23%)
Age (years old)	22.61 ± 3.88	46.64 ± 12.7	48.52 ± 13.1	45.36 ± 10.8	44.69 ± 14.0
Height (m)	1.71 ± 0.09	1.70 ± 0.1	1.72 ± 0.1	1.69 ± 0.1	1.72 ± 0.08
Weight (kg)	65.28 ± 10.77	70.84 ± 13.3	73.92 ± 12.4	64.05 ± 12.0	71.64 ± 14.6
Left cycle length (nb. points)	107.4 ± 6.7	220.5 ± 125.0	229.3 ± 142.5	209.2 ± 132.3	215.8 ± 92.6
Right cycle length (nb. points)	107.3 ± 6.6	222.8 ± 131.9	234.0 ± 157.3	209.7 ± 128.2	215.8 ± 91.8

a common limitation: they quantify the asymmetry based on global descriptors of gait, and thus do not exploit all the dynamic information available in the recorded kinematic joint signals [3–9].

On the other hand, Crenshaw and Richards [27] proposed to characterize gait asymmetry through personalized Singular Value Decomposition (SVD), to compare time-normalized left and right gait cycles, combined to linear regression. If the regression line is aligned with the first eigenvector, then gait is considered symmetrical, otherwise, there is an asymmetry. This measure thus quantifies globally the deviation from the regression line.

All these measures of asymmetry exploit normalized gait cycles or rely on the extraction of global features, thereby losing temporal information conveyed in gait waveforms [1,28]. By contrast, our work introduces a novel measure of gait asymmetry accounting for the relative spatiotemporal dynamics of both lower limbs. Also, we evaluate it across different motor impairments due to neurological diseases. In this respect, in the literature, studies are often focused on specific groups or diseases, such as healthy subjects [24], patients with hemiplegia [19] or with stroke [20,21,23].

More precisely, we propose to assess gait symmetry in a novel framework, by switching from gait signal analysis to image analysis. Our goal is to represent the matching between gait signals of both lower limbs through an image that summarizes the mutual gait cycle dynamics and the coordination between both sides. Such image, called Bilateral Dissimilarity Map, represents a compact cartography of the spatiotemporal relation between left and right gait cycles. Indeed, it conveys precious information on time shifts between left and right gait signals, as well as differences in their amplitudes.

Then, methodologically, we construct a model of normal gait using SVD on Bilateral Dissimilarity Maps of healthy controls. The SVD provides a compressed view of normal gait, through different eigenvector components that we exploit to compute an asymmetry index, referred as Eigen-Gait Asymmetry Index. We demonstrate that this index allows a fine assessment of gait asymmetry in patients with hemiparesis, tetraparesis and paraparesis.

The paper is structured as follows. Section 2 describes the Coubert Rehabilitation Center database and the acquisition protocol, as well as the method proposed in this work. The results are presented in Section 3 and discussed in Section 4. Conclusion and future work are finally stated in Section 5.

2. Materials and methods

2.1. Participants and acquisition protocol

We exploited angular kinematic data of 52 healthy subjects and 45 patients suffering from neurological diseases. Data was collected at the Movement Analysis Laboratory of Coubert Rehabilitation Center, at UGECAM Ile-de-France. Each participant was informed that his/her data might be used for research purposes, and no participant objected to the use of his/her data. This retrospective study was approved on April 10th, 2019 by the internal ethics committee of UGECAM Ile-de-France.

The acquisition was carried out during a spontaneous gait task using a Codamotion optoelectronic system, integrating four CX1 cameras. The
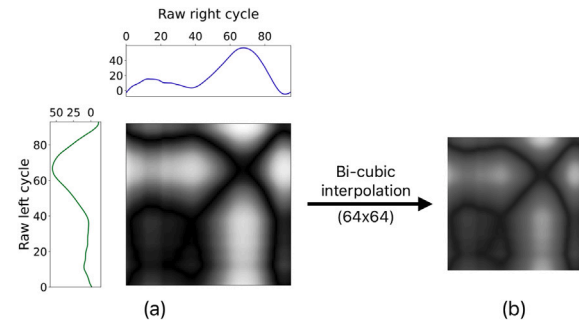

Fig. 1. BiDM construction: (a) a dissimilarity image matching two raw cycles of a healthy subject: the left cycle of length 94 and the right one of length 96; (b) the corresponding 64 × 64 BiDM image after bi-cubic interpolation. Each pixel in the image represents the Euclidean distance value between an observation from the left cycle and an observation from the right cycle.

system recovers 3D angular kinematics of pelvis, hip, foot, ankle, and knee in the sagittal, frontal and transversal planes, considering a sampling rate of 100 Hz. Participants were asked to walk naturally for 10 meters in a straight line and on flat ground with a spontaneous speed. This process was repeated five times in average, each corresponding to one gait trial.

The recruited healthy subjects (Healthy Controls, HC) were young adults (students or laboratory staff) ranging from 18 to 41 years old. They had no disease affecting motor function. Patients were adults ranging from 21 to 75 years old. Table 1 reports more details on the population under study. Among the 45 patients, 21 patients have hemiparesis (HP), 13 patients have incomplete tetraparesis (TP), and 11 patients have paraparesis (PP).

2.2. Data preprocessing and dissimilarity map construction

Joint angular kinematic signals were segmented into gait cycles from consecutive initial contacts events. Events were automatically detected using the High-Pass algorithm [29] and manually verified by a clinician specialized in movement analysis. The number of cycles differs for each trial and patient.

For symmetry assessment, we select for both HC and patients consecutive left and right gait cycles of the same individual and associate them as being a pair of bilateral gait cycles. This pair is then used to construct a dissimilarity matrix containing the Euclidean distance values computed between every observation in the left cycle and every observation in the right cycle (see Fig. 1a).

Note that by contrast to previous works [15–27,30–32], in this study we consider raw gait cycles without time normalization. Indeed, we have shown in [33,34] that normalizing cycles leads to significant spatiotemporal information loss. For this reason, we construct the dissimilarity matrix on raw cycles, and thus consider all spatiotemporal relations between left and right cycles. Consequently, the dissimilarity matrix is constructed based on the matching of two raw signals with different lengths. Then, we transform it into a 64 × 64 grey-scale image using bi-cubic interpolation (see Fig. 1b). This interpolation step was

studied in terms of image resolution and the method used. Experiments showed that bi-cubic interpolation at a resolution of 64×64 preserves the spatiotemporal pattern that emerged in the dissimilarity image, while reducing the risk of local distortions as well as computational cost. The resulting normalized grey-scale image is denoted in the following as "Bilateral Dissimilarity Map" (BiDM): it consists in a compact cartography of local matchings between left and right gait cycles (see Fig. 1b).

In order to enrich the dataset, we construct both "left vs. right" and "right vs. left" dissimilarity maps for each participant. The resulting "left vs. right" and "right vs. left" maps may convey different patterns for patients. Thereby, a total of 526 BiDMs result for HC, 200 for HP, 98 for PP, and 126 for the incomplete TP patients (424 BiDMs in total for patients).

2.3. Eigen-Gait asymmetry index

To characterize the asymmetry in patients, we adopt the following methodology in three steps:

1. Apply SVD on the BiDMs of the HC to retrieve eigenvectors synthesizing the symmetry patterns present in gait. Such eigenvectors define the principal directions of symmetric normal gait, namely the Eigen-Gait components;
2. Compute an average normal gait reference vector in the new space defined by Eigen-Gait components;
3. Project the BiDMs of HC and pathological individuals on this new space, and compute the distance to the average normal gait reference above-mentioned (in step 2), resulting in an Eigen-Gait Asymmetry Index (EGAI).

More precisely, we train the SVD on 80% of BiDMs of HC (i.e. 420 among 526 images) to extract the m Eigen-Gait components denoted $F_k, (k = 1, \ldots, m)$.

The projected BiDM $\widetilde{G}^m$ of the original one G is obtained as follows :

$$\widetilde{G}^m = \sum_{k=1}^{m} c_G^k . F_k \quad \text{with} \quad c_G^k = \langle G; F_k \rangle \tag{1}$$

where c_G^k is the contribution of G on the kth Eigen-Gait component, i.e. its associated coordinate on the kth principal direction.

The number of Eigen-Gait components m is chosen for each image so that $\widetilde{G}^m$ is the reconstructed image of G with at least 98%:

$$\Phi = \frac{\langle G; \widetilde{G}^m \rangle}{\|G\|^2} > 98\% \tag{2}$$

Finally, for the remaining 20% of BiDMs of HC (i.e. 106 among 526 images) and BiDMs of patients (200 for HP, 98 for PP and 126 for TP), we compute the EGAI associated to each BiDM (G) as follows:

$$EGAI(G) = \|c_G - \bar{c}_{HC}\| \text{ where } c_G = [c_G^1, \ldots, c_G^m]$$
$$\text{and } \bar{c}_{HC} = [\bar{c}_{HC}^1, \ldots, \bar{c}_{HC}^m] \tag{3}$$

where c_G is the contribution vector of G on the m Eigen-Gait components and $\bar{c}_{HC}$ is the average normal gait reference vector.

2.4. Comparison to DTW-based asymmetry score

An alternative approach to finely quantify gait asymmetry is to compute the Dynamic Time Warping (DTW) distance between left and right raw cycles, as recently done in [35,36]. This method entails identifying the optimal path within the dissimilarity matrix (i.e. dissimilarity image) and subsequently calculating the cumulative distance along this path, as displayed in Fig. 2 (the optimal path is represented in white).

DTW is a technique employed to align and compare two signals with different lengths. The method determines the optimal warping path that minimizes the cumulative distance between corresponding points in the
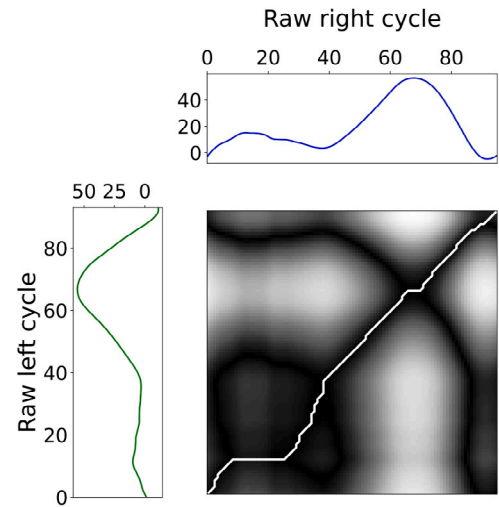

Fig. 2. Example of a dissimilarity image in which the optimal warping path (white line around the diagonal) is searched to compute DTW distance between left and right gait cycles. Each pixel in the image represents the Euclidean distance between an observation from the left cycle and an observation from the right one.

two signals. The DTW distance can be mathematically represented as shown in Eq. (4):

$$DTW_q(x, y) = \min_{\pi \in A(x,y)} \left\{ \left(\sum_{(i,j) \in \pi} \left| x_i - y_j \right|^q \right)^{\frac{1}{q}} \right\} \tag{4}$$

Here, $A(x, y)$ denotes the set of all feasible warping paths that adhere to the boundary conditions (i.e., the initial and final points of x and y are aligned) and monotonicity (i.e., the warping path does not regress in time). In this study, we fix $q = 2$ within the DTW algorithm, enabling the calculation of the Euclidean distance between the points along the optimal warping path. By utilizing DTW, we can attain a more accurate comparison of the signals, as it accounts for any temporal distortions or variations that may be present.

2.5. Statistical analysis

To evaluate the differences between groups, we use non-parametric statistical tests due to their ability in handling values that may not meet the assumptions of parametric tests, such as normality and homoscedasticity.

2.5.1. Kruskal–Wallis test

It is used to determine if there are statistically significant differences between the medians of more than two independent groups [37]. The test statistic H is calculated as follows:

$$H = \frac{12}{N(N+1)} \sum_{i=1}^{k} \frac{R_i^2}{n_i} - 3(N+1) \tag{5}$$

where, N is the total number of cycles in the database, k is the number of groups (here $k = 4$: HC, HP, PP and TP), R_i is the sum of the ranks in the ith group, and n_i is the number of cycles in the ith group.

2.5.2. Mann–Whitney test

It assesses whether the distributions of two independent groups of values are identical [38]. The test statistic U is given by:

$$U = n_1 n_2 \min\left\{ \frac{n_1(n_1+1)}{2} - R_1; \frac{n_2(n_2+1)}{2} - R_2 \right\} \tag{6}$$

where, n_1, n_2 are the number of cycles within the two groups, and R_1, R_2 are the sums of the ranks for the two groups.
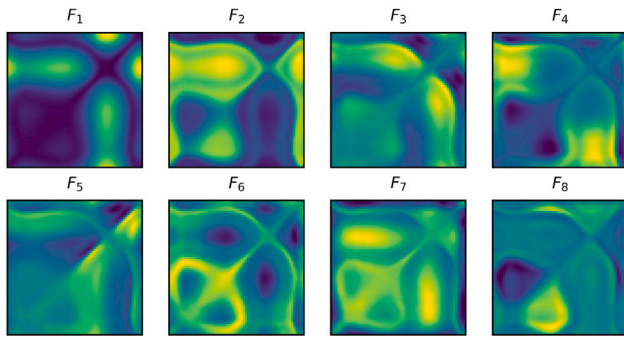
Fig. 3. The top eight singular vectors obtained on 80% of BiDMs of HC. In order to ease the visualization, the grey-scale colormap is replaced by the viridis colormap, so that whites are replaced by yellows and blacks are replaced by dark blues.

2.5.3. Cliff's delta statistic

To quantify the degree of overlap between two groups, we use the non-parametric effect size measure, namely Cliff's delta (δ) [39]:

$$\delta = \frac{\mathrm{Card}\{x_i > x_j\} - \mathrm{Card}\{x_i < x_j\}}{n_1 n_2} \tag{7}$$

where, x_i and x_j are the values within two different groups, and n_1, n_2 are the number of cycles within the two groups. Cliff's delta ranges from -1 to 1; values close to 0 indicate a high degree of overlap between groups, and values close to -1 or 1 indicate a low degree of overlap.

3. Experiments and results

3.1. EGAI analysis on the sagittal knee angle

We started experiments considering only the knee joint in the sagittal plane. We performed the SVD as previously explained by choosing m, the number of Eigen-Gait components, for each image according to Eq. (2).

Results showed that BiDMs of HP patients require a very high value of m in average ($m = 405$) to be reconstructed with good quality. Also, we found that the TP group shows a high value of m in average ($m = 115$). Finally, the number of Eigen-Gait components doubles for the PP group ($m = 231$) comparatively to incomplete TP. By contrast, we found that BiDMs of HC require, as expected, a very small number of Eigen-Gait components ($m = 2$). These first results show the pertinence of our approach that exploits SVD on BiDMs for building a model of normal symmetric gait characterized by Eigen-Gait components.

For a better insight into the Eigen-Gait components extracted during training, we display in Fig. 3 the resulting top eight Eigen-Gait components for the HC group. We remark that some of these maps are symmetric about the first bisectors (F_1, F_3, F_4, F_6 and F_7) whereas others are non-symmetric (F_2, F_5, F_8). The first components convey the symmetry existing in normal gait; however, it is still interesting to extend to more components to represent the variance existing in symmetry among normal gait patterns. Consequently, given the high heterogeneity among patients, more components are required to reconstruct with enough quality their corresponding BiDMs.

Thus, to study in the sequel the potential use of EGAI for asymmetry assessment in HC, HP, PP and TP, we construct all the BiDMs of HC (526 images) and those of patients (424 images) with m fixed to 156. This value corresponds to the average number of Eigen-Gait components required to reconstruct with good quality the images of the test subset (containing the 20% remaining of HC BiDMs and all the BiDMs of patients).

Fig. 4 displays the sagittal knee EGAI values per patient computed for all his/her associated BiDMs, as indicated in Eq. (3). We notice that the EGAI values of patients are in general much higher (9.73 ±2.16)
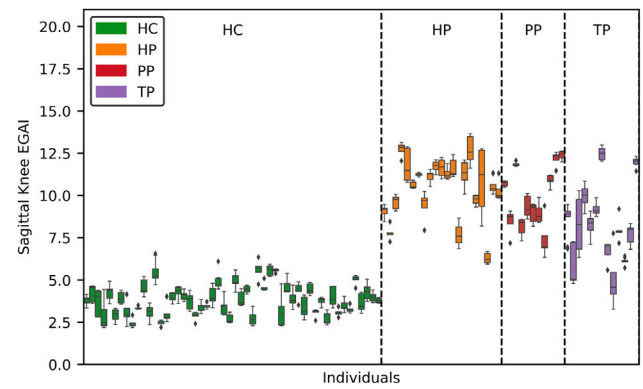

Fig. 4. EGAI values for each individual (HC in green, HP in orange, PP in red and TP in purple) considering the knee sagittal angle. Each boxplot represents intra-personal variance of EGAI values across cycles (BiDMs).
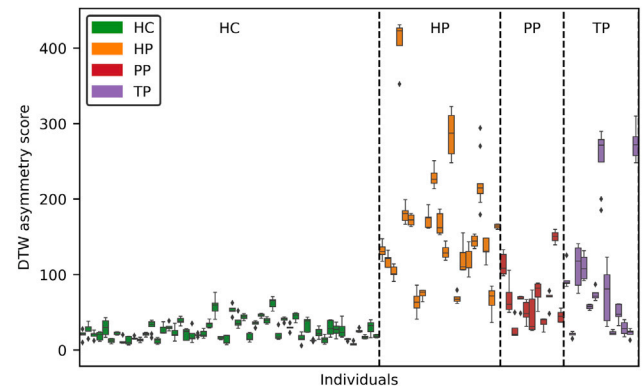

Fig. 5. DTW asymmetry score for each individual (HC in green, HP in orange, PP in red and TP in purple) computed between his/her left and right cycles, considering the knee sagittal angle.

than those of HC (3.86 ±0.9), reflecting the asymmetry induced by neurological diseases.

The statistical analysis using the Kruskal–Wallis test indicates a significant difference among groups ($p = 8 \cdot 10^{-150}$). For pairwise comparisons, the Mann–Whitney test reveals significant differences between HC and patients: $p = 3 \cdot 10^{-96}$ for HC vs. HP, $p = 1 \cdot 10^{-55}$ for HC vs. PP and $p = 3 \cdot 10^{-61}$ for HC vs. TP. For a deeper analysis, the Cliff's delta values indicate a very low degree of overlap between HC and patients, with HC group showing lower EGAI values than patients ($\delta = -0.99$ for HC vs. HP, $\delta = -0.99$ for HC vs. PP and $\delta = -0.95$ for HC vs. TP).

Moreover, patients with hemiparesis show the highest EGAI (10.4 ±1.8), followed by patients with paraparesis (9.9 ±1.8) and patients with tetraparesis (8.6 ±2.5). Indeed, patients with hemiparesis show a more asymmetrical gait since only one side of the body is affected. The Mann–Whitney test also shows significant differences ($p< 0.05$) between pairs of patients' groups (HP vs. PP, HP vs. TP and PP vs. TP).

Furthermore, HC show less variance of their EGAI values across cycles than patients. Also, subjects presenting more variance in their EGAI are among pathological populations, especially patients with HP and TP.

3.2. Comparative analysis between EGAI and a DTW-based asymmetry score

Fig. 5 shows that measuring gait asymmetry using the DTW score (as described in Section 2.4) is less effective than using the EGAI (see Fig. 4).
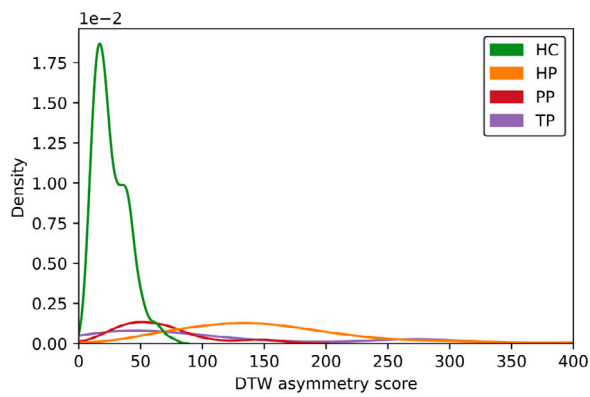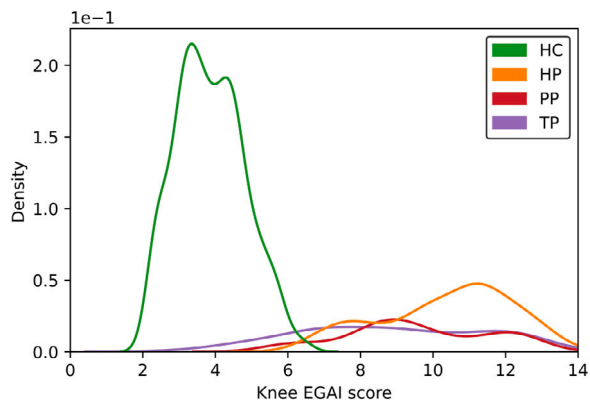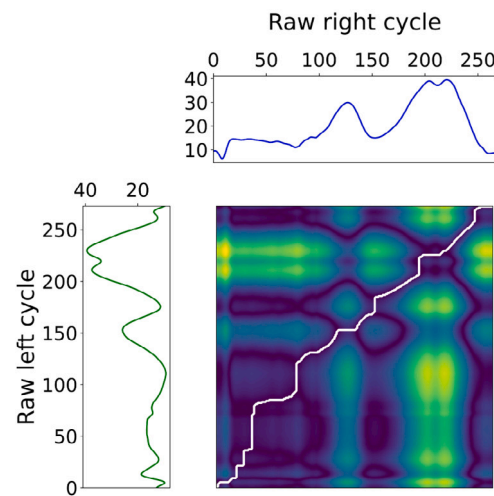
Fig. 6. Asymmetry score distributions considering the knee sagittal angle, for HC (in green), HP (in orange), PP (in red) and TP (in purple) with: (a) DTW and (b) EGAI.
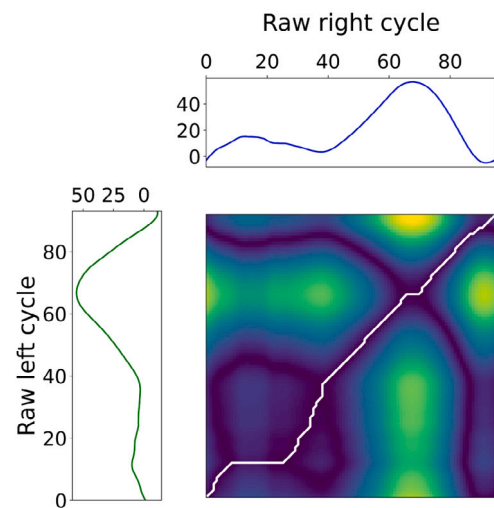

Fig. 7. Example of a dissimilarity image of: (a) a patient with low DTW-based score and high EGAI score; (b) a healthy subject. In order to ease the visualization, the grey-scale colormap is replaced by the viridis colormap, so that whites are replaced by yellows and blacks are replaced by dark blues.

Notably, several pathological cycles from the HP group, and particularly from the PP and TP groups, exhibit DTW asymmetry scores within the same range as those of HC. This is illustrated more precisely in Fig. 6 that displays the distributions of the DTW score and EGAI across the four groups. The overlap between healthy subjects and patients is higher with DTW score (Fig. 6(a)) than with EGAI (Fig. 6(b)). This is supported by the statistical analysis. The Mann–Whitney test indicates a significant difference between HC and each group of patients with DTW score. Nevertheless, compared to EGAI, the absolute values of Cliff's delta calculated between HC and patients are found lower with DTW ($\delta = -0.94$ for HC vs. HP, $\delta = -0.83$ for HC vs. PP and $\delta = -0.69$ for HC vs. TP).

Besides, the overlap also increases between patients with TP and PP using DTW. This is confirmed by the Mann–Whitney test, which shows no significant difference between TP and PP for the DTW score ($p = 0.79$), in contrast to the EGAI ($p = 3.10^{-5}$).

Furthermore, we remark that some bilateral gait cycles have a low DTW-based asymmetry score while having a high EGAI score. This phenomenon appears for some patients, as shown in Fig. 7(a). The left and the right gait cycles of this person are very similar, leading to a DTW path (plotted in white) close to the diagonal of the dissimilarity map, and therefore to a low DTW score. By contrast, the BiDM of this person shows a bilateral pattern that completely differs from that of normal gait (see Fig. 7(b)), which explains the high EGAI score. This confirms that our innovative approach enables a fine characterization of bilateral gait asymmetry through BiDMs.

3.3. EGAI analysis on the other joint kinematics

We extend our gait asymmetry analysis using EGAI to encompass additional joints, focusing on the sagittal plane since our analyses on other planes did not yield significant findings. For this reason, Fig. 8 presents EGAI results for HC, HP, PP, and TP groups in the sagittal plane only. To facilitate comparisons across different joints, EGAI values were scaled between 0 and 1.

We observe that HC present the lowest EGAI values for the four joints, especially for the knee, the ankle, and the hip. Globally, we note for pathological groups a trend of higher EGAI values for HP and lower values for incomplete TP. The behavior of EGAI values in PP patients is more variable depending on the considered joint: for the knee and the ankle, there is an important overlap between EGAI values of PP and HP, and for the pelvis, there is an important overlap between PP and TP. Finally, we notice that the ankle does not allow distinguishing HP, PP and TP in terms of asymmetry.
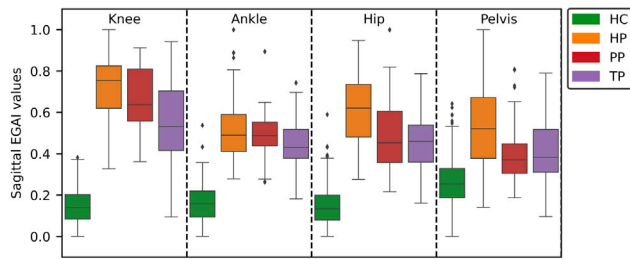
Fig. 8. Boxplots of EGAI values for HC, HP, PP, and TP populations considering knee, ankle, hip and pelvis angular kinematics in the sagittal plane.
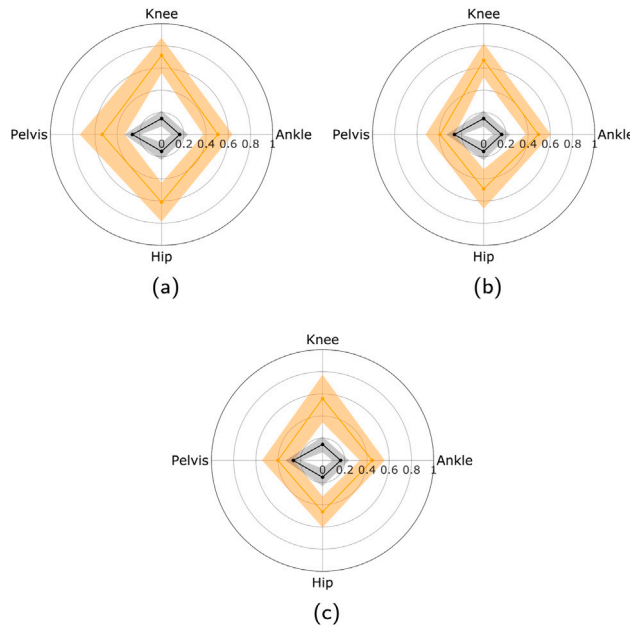

Fig. 9. Average EGAI radar charts of: (a) HP, (b) PP and (c) TP patients (in orange). The average EGAI for HC is represented in black. Each radar chart is composed of average EGAI values and standard deviations for the knee, ankle, hip and pelvis in the sagittal plane.

Fig. 10. Examples of radar charts for four HP patients: (a) Patient 0, (b) Patient 2, (c) Patient 28 and (d) Patient 30. Average radar chart of HC subjects is represented in black.

Fig. 11. Examples of radar charts for four PP patients: (a) Patient 5, (b) Patient 6, (c) Patient 27 and (d) Patient 33. Average radar chart of HC subjects is represented in black.

For a holistic understanding on gait impairments across multiple joints, we plot in Fig. 9 radar charts for HP, PP and TP patients separately, by representing in orange the average EGAI scores obtained on the knee, ankle, hip, and pelvis kinematics in the sagittal plane. On the same radar charts, we report in black the average EGAI scores of HC.

The trend observed in Fig. 8 is confirmed in Fig. 9, where the average profile of HP patients (Fig. 9(a)) is more distant from the average profile of HC (displayed in black) than that of PP (Fig. 9(b)) and TP patients (Fig. 9(c)). This finding underscores the suitability of our approach for characterizing asymmetry in each joint in the sagittal plane. To provide a more comprehensive visualization, we present examples of radar charts for some selected HP patients in Fig. 10, some PP patients in Fig. 11, and some TP patients in Fig. 12. Actually, our proposed method allows assessing gait asymmetry and deviation from normal gait for a patients' group, as well as for an individual.

4. Discussion

In the present study, we introduced a novel metric, referred to as EGAI, for quantifying gait asymmetry in patients with HP, PP and TP. Our method relies on the matching between raw gait cycles of both lower limbs using a Bilateral Dissimilarity Map image. Such image, denoted BiDM, conveys a rich information content: the mutual gait
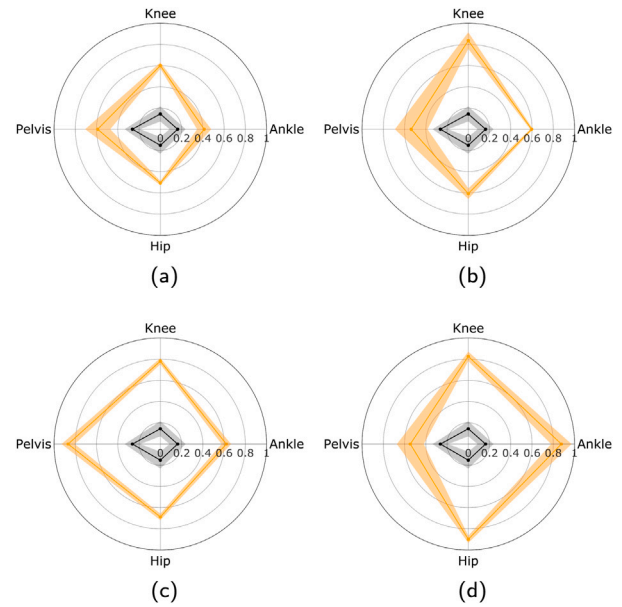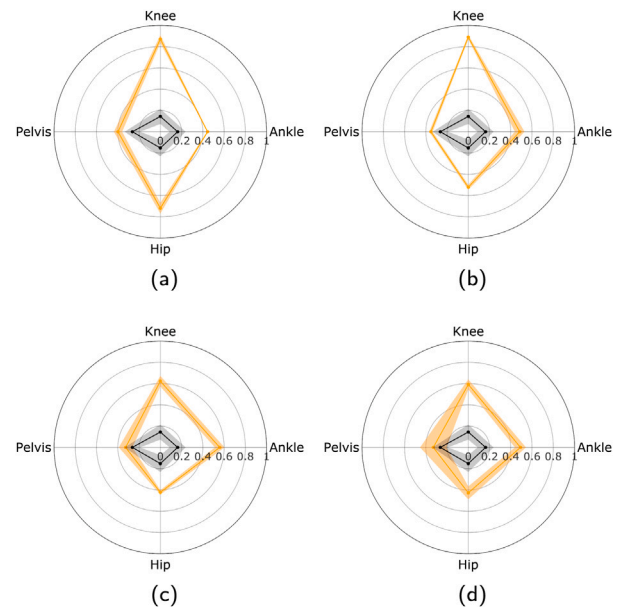
dynamics and the coordination between both sides. Then, using SVD, we built a model of normal gait considering BiDMs of HC. By projecting the dissimilarity maps of other HC (20% of the healthy population) as well as HP, PP, and TP patients on the space of singular vectors, we computed the EGAI.

Considering only the knee joint in the sagittal plane, experiments have shown that BiDMs of HC require a very small number of Eigen-Gait components ($m = 2$) to be reconstructed with good quality. On the contrary, dissimilarity maps of TP require a high value of m ($m = 115$), which doubles for the PP group ($m = 231$), and reaches the highest value for the HP group ($m = 405$). These results reveal that our approach allows quantifying the asymmetry in bilateral gait for
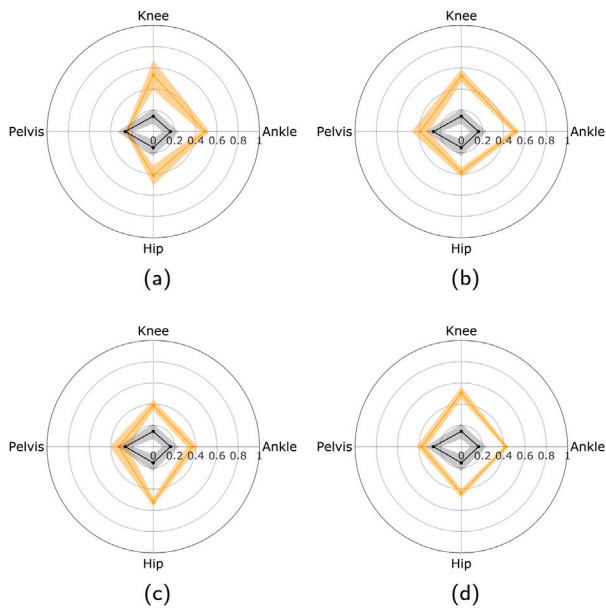
Fig. 12. Examples of radar charts for four TP patients: (a) Patient 12, (b) Patient 16, (c) Patient 22 and (d) Patient 38. Average radar chart of HC subjects is represented in black.

patients, according to the type of motor impairment. More precisely, since the singular vectors are estimated only on HC, by projecting patients on this space, the EGAI is able to quantify the deviation from normal gait symmetry. Indeed, more Eigen-Gait components are required when the deviation from normal gait increases. From this point of view, the HP population exhibits the highest asymmetry. These first observations on m values were also confirmed by EGAI values of HC and patients: EGAI of HP, PP and TP are much higher in average (9.73 ± 2.16) than those of HC (3.86 ± 0.9). The statistical analysis showed significant differences between all groups' pairs ($p < 0.05$). Also, HC show less variance of their EGAI values across cycles than patients: this is consistent with their better motor control and coordination of lower limb movements. All these results demonstrate the effectiveness of our approach in finely quantifying gait asymmetry in patients according to their motor impairment.

By comparing the ability of EGAI versus DTW distance to assess gait asymmetry [35,36], we found that the DTW-based asymmetry score was not able to differentiate well HC cycles from pathological ones, contrary to EGAI. Indeed, several cycles from the HP group, and particularly from the PP and TP groups show DTW asymmetry scores within the same range as those of HC (Fig. 5 versus Fig. 4, and Fig. 6). Specifically, the absolute value of the Cliff's delta calculated between HC and each patient group was found much higher with the EGAI approach than with DTW. Besides, the statistical analysis did not reveal a significant difference between TP and PP with DTW-based score ($p = 0.79$). This can be explained by the fact that the DTW-based asymmetry score relies only on one matching (the optimal path) between left and right cycles, whereas the EGAI is based on the BiDM that incorporates all possible matchings between left and right cycles.

This interesting finding underlines the importance of considering all local matchings between left and right gait cycles to quantify gait asymmetry. Indeed, this new paradigm provides a comprehensive view on the spatiotemporal coordination of lower limbs. Additionally, with SVD, we can further break down the dissimilarity maps into their most essential information, represented by Eigen-Gait components. Both aspects contribute to a refined understanding of gait symmetry.

To provide a complete assessment of gait, the EGAI has been calculated for the knee, ankle, hip, and pelvis on the sagittal plane. Fig. 8 showed that patients exhibit high EGAI values compared to HC for all

joints. Also, HP patients exhibit the highest EGAI scores for all joints, which reflects a pronounced gait asymmetry in all joints due to the unilateral impact of the impairment. We obtained lower EGAI scores in the TP group for most joints, and observed that the EGAI in the PP group has an intermediate behavior depending on the joint.

Our results demonstrated the efficiency of the proposed EGAI in quantifying the degree of asymmetry induced by motor impairments. Our metric offers a holistic evaluation of gait achieving two key innovations: (i) the construction of dissimilarity maps capturing the spatiotemporal deviations between the left and right lower limbs; (ii) the application of SVD to extract Eigen-Gait components that encapsulate the spatiotemporal characteristics of symmetry in normal gait.

However, some limitations remain. These first results were obtained on a dataset containing young healthy adults. It would be interesting to include a healthy population spanning a larger variety of ages for a better representation of the existing variance in normal gait. Moreover, we have few patients per motor impairment; also, there is an imbalance in the number of patients across motor impairments. This necessitates conducting our study on an extended dataset to confirm the obtained trends.

5. Conclusion

In this study, we proposed a novel framework for quantifying gait asymmetry, by switching from gait signal analysis to image analysis. Such image (BiDM) represents the matching between gait signals of both lower limbs, summarizing the mutual gait cycle dynamics. By exploiting SVD on BiDMs of HC, we extracted the essential information in normal gait symmetry, encoded by Eigen-Gait components. We proposed to measure the specific deviation of each motor impairment (HP, PP, and TP) with regard to normal gait symmetry via the EGAI. A personalized analysis pointed out the progressive decrease of EGAI from patients with hemiparesis, to those with paraparesis and finally to those with tetraparesis. The most pronounced asymmetry is thus shown in patients with hemiparesis.

In subsequent research, we aim at exploring the impact of considering a personalized number of Eigen-Gait components for evaluating gait asymmetry. Indeed, our study has uncovered a gradual decrease in the number of required components from HP (with the highest values) to PP, and finally to TP, to well reconstruct BiDMs. Furthermore, we intend to investigate the potential application of the EGAI for assessing the effectiveness of therapeutic interventions in future studies.

Declaration of competing interest

The authors declare that they have no known competing financial interests or personal relationships that could have appeared to influence the work reported in this paper.

References

[1] S. Viteckova, P. Kutilek, Z. Svoboda, R. Krupicka, J. Kauler, Z. Szabo, Gait symmetry measures: A review of current and prospective methods, Biomed. Signal Process. Control 42 (2018) 89–100, http://dx.doi.org/10.1016/j.bspc.2018.01.013.

[2] K.K. Patterson, I. Parafianowicz, C.J. Danells, V. Closson, M.C. Verrier, W.R. Staines, S.E. Black, W.E. McIlroy, Gait asymmetry in community-ambulating stroke survivors, Arch. Phys. Med. Rehabil. 89 (2) (2008) 304–310, http://dx.doi.org/10.1016/j.apmr.2007.08.142, Publisher: Elsevier.

[3] M. Błażkiewicz, A. Wit, Artificial neural network simulation of lower limb joint angles in normal and impaired human gait, Acta Bioeng. Biomech. 20 (2018) 43–49, http://dx.doi.org/10.5277/ABB-01129-2018-02.

[4] T.P. Luu, K.H. Low, X. Qu, H.B. Lim, K.H. Hoon, An individual-specific gait pattern prediction model based on generalized regression neural networks, Gait Posture 39 (1) (2014) 443–448, http://dx.doi.org/10.1016/j.gaitpost.2013.08.028.

[5] S. Sivakumar, A. Gopalai, K.H. Lim, D. Gouwanda, Artificial neural network based ankle joint angle estimation using instrumented foot insoles, Biomed. Signal Process. Control 54 (2019) 101614, http://dx.doi.org/10.1016/j.bspc.2019.101614.

[6] M. Sharifi Renani, A.M. Eustace, C.A. Myers, C.W. Clary, The use of synthetic IMU signals in the training of deep learning models significantly improves the accuracy of joint kinematic predictions, Sensors 21 (17) (2021) 5876, http://dx.doi.org/10.3390/s21175876.

[7] B. Stetter, F. Krafft, S. Ringhof, T. Stein, S. Sell, A machine learning and wearable sensor based approach to estimate external knee flexion and adduction moments during various locomotion tasks, Front. Bioeng. Biotechnol. 8 (2020) http://dx.doi.org/10.3389/fbioe.2020.00009.

[8] G. Giarmatzis, E.I. Zacharaki, K. Moustakas, Real-time prediction of joint forces by motion capture and machine learning, Sensors 20 (23) (2020) 6933, http://dx.doi.org/10.3390/s20236933.

[9] F.J. Wouda, M. Giuberti, G. Bellusci, P.H. Veltink, Estimation of full-body poses using only five inertial sensors: An eager or lazy learning approach? Sensors 16 (12) (2016) 2138, http://dx.doi.org/10.3390/s16122138.

[10] R. Argent, S. Drummond, A. Remus, M. O'Reilly, B. Caulfield, Evaluating the use of machine learning in the assessment of joint angle using a single inertial sensor, J. Rehabil. Assist. Technol. Eng. 6 (2019) http://dx.doi.org/10.1177/2055668319868544.

[11] J. Chen, X. Zhang, Y. Cheng, N. Xi, Surface EMG based continuous estimation of human lower limb joint angles by using deep belief networks, Biomed. Signal Process. Control 40 (2018) 335–342, http://dx.doi.org/10.1016/j.bspc.2017.10.002.

[12] S. Farmer, S. Silver-Thorn, P. Voglewede, S.A. Beardsley, Within-socket myoelectric prediction of continuous ankle kinematics for control of a powered transtibial prosthesis, J. Neural Eng. 11 (5) (2014) http://dx.doi.org/10.1088/1741-2560/11/5/056027.

[13] A. Findlow, J.Y. Goulermas, C. Nester, D. Howard, L.P.J. Kenney, Predicting lower limb joint kinematics using wearable motion sensors, Gait Posture 28 (1) (2008) 120–126, http://dx.doi.org/10.1016/j.gaitpost.2007.11.001.

[14] W. Zeng, C. Yuan, Q. Wang, F. Liu, Y. Wang, Classification of gait patterns between patients with Parkinson's disease and healthy controls using phase space reconstruction (PSR), empirical mode decomposition (EMD) and neural networks, Neural Netw.: Off. J. Int. Neural Netw. Soc. 111 (2019) 64–76, http://dx.doi.org/10.1016/j.neunet.2018.12.012.

[15] V. Cimolin, M. Galli, Summary measures for clinical gait analysis: a literature review, Gait Posture 39 (4) (2014) 1005–1010, http://dx.doi.org/10.1016/j.gaitpost.2014.02.001.

[16] H.L. Siebers, W. Alrawashdeh, M. Betsch, F. Migliorini, F. Hildebrand, J. Eschweiler, Comparison of different symmetry indices for the quantification of dynamic joint angles, BMC Sports Sci. Med. Rehabil. 13 (1) (2021) 130, http://dx.doi.org/10.1186/s13102-021-00355-4.

[17] S. Ganguli, P. Mukherji, K.S. Bose, Gait evaluation of unilateral below-knee amputees fitted with patellar-tendon-bearing prostheses, J. Indian Med. Assoc. 63 (8) (1974) 256–259.

[18] R.O. Robinson, W. Herzog, B.M. Nigg, Use of force platform variables to quantify the effects of chiropractic manipulation on gait symmetry, J. Manipulative Physiol. Ther. 10 (4) (1987) 172–176.

[19] C.K. Balasubramanian, M.G. Bowden, R.R. Neptune, S.A. Kautz, Relationship between step length asymmetry and walking performance in subjects with chronic hemiparesis, Arch. Phys. Med. Rehabil. 88 (1) (2007) 43–49, http://dx.doi.org/10.1016/j.apmr.2006.10.004.

[20] P.-Y. Lin, Y.-R. Yang, S.-J. Cheng, R.-Y. Wang, The relation between ankle impairments and gait velocity and symmetry in people with stroke, Arch. Phys. Med. Rehabil. 87 (4) (2006) 562–568, http://dx.doi.org/10.1016/j.apmr.2005.12.042.

[21] A.-L. Hsu, P.-F. Tang, M.-H. Jan, Analysis of impairments influencing gait velocity and asymmetry of hemiplegic patients after mild to moderate stroke, Arch. Phys. Med. Rehabil. 84 (8) (2003) 1185–1193, http://dx.doi.org/10.1016/s0003-9993(03)00030-3.

[22] S. Hesse, C. Werner, H. Seibel, S. von Frankenberg, E.-M. Kappel, S. Kirker, M. Käding, Treadmill training with partial body-weight support after total hip arthroplasty: a randomized controlled trial, Arch. Phys. Med. Rehabil. 84 (12) (2003) 1767–1773, http://dx.doi.org/10.1016/s0003-9993(03)00434-9.

[23] S. Bovonsunthonchai, V. Hiengkaew, R. Vachalathiti, M. Vongsirinavarat, Gait symmetrical indexes and their relationships to muscle tone, lower extremity function, and postural balance in mild to moderate stroke, J. Med. Assoc. Thai. 94 (4) (2011) 476–484.

[24] K. Jansen, F. De Groote, J. Duysens, I. Jonkers, Muscle contributions to center of mass acceleration adapt to asymmetric walking in healthy subjects, Gait Posture 38 (4) (2013) 739–744, http://dx.doi.org/10.1016/j.gaitpost.2013.03.013.

[25] K. Orlowski, H. Loose., F. Eckardt., J. Edelmann-Nusser., K. Witte., Analyzing the transfemoral amputee gait using inertial sensors - identifying gait parameters for investigating the symmetry of gait - a pilot study, in: Proceedings of the International Conference on Bio-Inspired Systems and Signal Processing (BIOSTEC 2015) - BIOSIGNALS, SciTePress, INSTICC, 2015, pp. 258–263, http://dx.doi.org/10.5220/0005250802580263.

[26] R.A. Zifchock, I. Davis, J. Higginson, T. Royer, The symmetry angle: a novel, robust method of quantifying asymmetry, Gait Posture 27 (4) (2008) 622–627, http://dx.doi.org/10.1016/j.gaitpost.2007.08.006.

[27] S.J. Crenshaw, J.G. Richards, A method for analyzing joint symmetry and normalcy, with an application to analyzing gait, Gait Posture 24 (4) (2006) 515–521, http://dx.doi.org/10.1016/j.gaitpost.2005.12.002.

[28] K. Deluzio, J. Astephen, Biomechanical features of gait waveform data associated with knee osteoarthritis: An application of principal component analysis, Gait Posture 25 (1) (2007) 86–93, http://dx.doi.org/10.1016/j.gaitpost.2006.01.007.

[29] E. Desailly, Y. Daniel, P. Sardain, P. Lacouture, Foot contact event detection using kinematic data in cerebral palsy children and normal adults gait, Gait Posture 29 (1) (2009) 76–80, http://dx.doi.org/10.1016/j.gaitpost.2008.06.009.

[30] M.H. Schwartz, A. Rozumalski, The gait deviation index: a new comprehensive index of gait pathology, Gait Posture 28 (3) (2008) 351–357, http://dx.doi.org/10.1016/j.gaitpost.2008.05.001.

[31] R. Baker, J.L. McGinley, M.H. Schwartz, S. Beynon, A. Rozumalski, H.K. Graham, O. Tirosh, The gait profile score and movement analysis profile, Gait Posture 30 (3) (2009) 265–269, http://dx.doi.org/10.1016/j.gaitpost.2009.05.020.

[32] A. Cretual, K. Bervet, L. Ballaz, Gillette Gait Index in adults, Gait Posture 32 (3) (2010) 307–310, http://dx.doi.org/10.1016/j.gaitpost.2010.05.015.

[33] L. Hermez, A. Halimi, N. Houmani, S. Garcia-Salicetti, O. Galarraga, V. Vigneron, Clinical gait analysis: Characterizing normal gait and pathological deviations due to neurological diseases, Sensors (Basel, Switzerland) 23 (14) (2023) 6566, http://dx.doi.org/10.3390/s23146566.

[34] L. Hermez, N. Houmani, S. Garcia-Salicetti, O. Galarraga, V. Vigneron, Gait deviation and neurological diseases: a comparative study of quantitative measures, in: 11th IEEE International Conference on E-Health and Bioengineering, EHB 2023, Bucharest, Romania, 2023.

[35] H. Zhao, H. Xu, Z. Wang, L. Wang, S. Qiu, D. Peng, J. Li, J. Jiang, Analysis and evaluation of hemiplegic gait based on wearable sensor network, Inf. Fusion 90 (2023) 382–391, http://dx.doi.org/10.1016/j.inffus.2022.10.003.

[36] M. Błażkiewicz, K. Lann Vel Lace, A. Hadamus, Gait symmetry analysis based on dynamic time warping, Symmetry 13 (5) (2021) 836, http://dx.doi.org/10.3390/sym13050836.

[37] W.H. Kruskal, W.A. Wallis, Use of ranks in one-criterion variance analysis, J. Amer. Statist. Assoc. 47 (260) (1952) 583–621, http://dx.doi.org/10.1080/01621459.1952.10483441.

[38] H.B. Mann, D.R. Whitney, On a test of whether one of two random variables is stochastically larger than the other, Ann. Math. Stat. 18 (1) (1947) 50–60, http://dx.doi.org/10.1214/aoms/1177730491.

[39] N. Cliff, Dominance statistics: Ordinal analyses to answer ordinal questions, Psychol. Bull. 114 (3) (1993) 494–509, http://dx.doi.org/10.1037/0033-2909.114.3.494.